# Comparison of magnetic anisotropy and structural properties in chemically ordered CoPt and FePt nanoparticles

Alexandre Tamion, Florent Tournus, Nils Blanc, Arnaud Hillion, O Proux, Andrei Rogalev, Fabrice Wilhelm, Véronique Dupuis, J. Gutierrez Valdes, Luis E. Diaz-Sanchez, et al.

# Comparison of magnetic anisotropy and structural properties in chemically ordered CoPt and FePt nanoparticles.

A. Tamion[1],* F. Tournus[1], N. Blanc[2], A. Hillion[3], O. Proux[4], A. Rogalev[5], F. Wilhelm[5], J. Gutierrez Valdes[6], L. E. Díaz-Sánchez[6], K. Sato[7], G. M. Pastor[8], and V. Dupuis[1]

[1] *Univ Lyon, Université Lyon 1, CNRS, Institut Lumière Matière UMR 5306, 69622 Villeurbanne, France*
[2] *Université Grenoble Alpes, CNRS, Grenoble INP, Institut Néel, 38000 Grenoble, France*
[3] *Université de Toulouse, LPCNO, INSA-CNRS-UPS, 135 avenue de Rangueil, Toulouse 31077, France*
[4] *Observatoire des Sciences de l'Univers, 38051 Grenoble, France*
[5] *European Synchrotron Radiation Facility, BP 220, 38043 Grenoble, France*
[6] *Universidad Autónoma del Estado de México, Faculty of Sciences, Toluca, México*
[7] *Institute for Materials Research, Tohoku University, Sendai 980-8577, Japan present address Research Center for Ultra-High Voltage Electron Microscopy, Osaka University, Ibaraki 567-0047, Japan and*
[8] *Institut für Theoretische Physik, Universität Kassel, 34132 Kassel, Germany*

(Dated: April 11, 2022)

The intrinsic magnetic properties of nanoparticles can be accurately determined using highly dispersed nanoparticles in a matrix. In this paper, we study chemically ordered CoPt and FePt nanoparticles with a diameter of 3 nm embedded in an amorphous carbon matrix. Although both alloys exhibit almost the same magnetic and crystallographic properties in the bulk materials, they are completely different as nanoparticles. We show that their magnetic anisotropy differs greatly. In order to understand the origin of such a difference a fine crystallographic structure study has been performed using EXAFS. In that respect, the atomic relaxations appear to be different in both nanoalloys. *Ab initio* calculations of the atomic relaxation shed light on these experimental results, showing that the wide distance distribution in Co sub-lattice should strongly alter the magnetic anisotropy of CoPt nanoparticles.

## I. INTRODUCTION

Magnetic nanoalloys are currently of great interest in a wide range of disciplines, including magnetic fluids, catalysis, biotechnology, biomedicine, magnetic resonance imaging, data storage, and environmental remediation [1–14]. In order to use magnetic nanoparticles in any kind of application it is necessary to know their magnetic properties, in particular their magnetic anisotropy energy. Otherwise, the small size of particles can be boon and bane, since the nanoparticles' magnetization direction can rapidly switch due to thermal fluctuations, which is the so-called superparamagnetic limit. The blocking temperature $T_{\mathrm{B}}$ is the parameter used to separate the blocked (low temperature) and the superparamagnetic regime (high temperature). $T_{\mathrm{B}}$ is directly proportional to the magnetic anisotropy energy $\Delta E$ which can be expressed in terms of the anisotropy constant $K$ and the particle volume $V$ through the well known following relation $T_{\mathrm{B}} \approx \Delta E/25\mathrm{k_B}$ with $\Delta E = KV$ [15].

In the bulk $L1_0$ phase CoPt and FePt alloys exhibit similar magnetic and structural properties [16]. Indeed, the tetragonalization of the unit cell as measured by the $c/a$ ratio is almost the same ($c/a \approx 0.97$) and their uniaxial anisotropy constants are $K_{CoPt} = 5$ MJ.m$^{-3}$ and $K_{FePt} = 7\ MJ.m^{-3}$ [17]. These extremely high uniaxial anisotropies are observed in the periodic solid due to the stacking of Co (or Fe) and Pt atomic planes along the (001) direction. In that respect, CoPt and FePt alloys in chemically ordered $L1_0$ phase, are some of the best candidates to reach a sufficiently high blocking temperature at the nanoscale, and thus to be used in magnetic applications.

In this context, there has been considerable progress in the synthesis procedures of FePt [11, 18] and CoPt [19–25] $L1_0$ nanoparticles. Chemical ordering is often obtained by annealing, which goes with problems of pollution or coalescence. As a consequence it is a very difficult task to ensure that chemically ordered nanoparticles do not coalesce and do not interact with each others.

The main goal of this work is then to determine and compare the intrinsic magnetic anisotropy constant of CoPt and FePt nanoparticles, and to understand the possible origin of any significant difference. For this purpose we have elaborated similar samples made of chemically ordered nanoparticles with negligible magnetic interactions. The present article is made up of six sections. After a section briefly describing the sample preparation

and demonstrating the negligible magnetic interactions between nanoparticles (section II), we verify, using high resolution transmission electron microscopy (TEM), the chemical ordering after annealing (section III). In section IV, the nanoparticles' intrinsic magnetic properties are accurately determined thanks to a global fit of various magnetic measurements.

The magnetic properties are then linked to the atomic structure using extented X-ray absorption fine structure (EXAFS) experiments and modeling in section V. Finally, the major influence of atomic relaxations is inferred from *ab-initio* calculations in section VI.

## II. SAMPLE PREPARATION

The alloy nanoparticles (NPs) are synthesized using the Mass Selected Low Energy Cluster Beam Deposition (MSLECBD) technique that allows us to grow thin films of pre-formed nanoparticles deposited on a substrate[26, 27]. In the following we give a short description of this technique. Clusters are produced in a laser vaporization-gas condensation source. First, a plasma is created by the impact of a Nd:YAG (yttrium-aluminum-garnet) laser beam focused on a CoPt or FePt rod, and thermalized by injection of a continuous flow of helium at low pressure (typically 30 mbar) which induces the NPs growth. Second, the NPs are stabilized and cooled down in the supersonic expansion which takes place at the exit nozzle of the source. NPs are Mass-selected by an electrostatic quadrupole, and transferred to an ultrahigh vacuum chamber (base pressure of $10^{-10}$ mbar) where they are deposited at low kinetic energy together with carbon atoms onto a carbon buffer. In this physical process, the mean cluster's composition is then directly the rod's composition . The distribution of composition is only statistical and depends on the number of atoms in the nanoparticles [28–31]. Whereas in FePt NPs prepared by chemical way, the $L1_0$ order cannot be achieved for particles smaller than 3 nm [32], in physical way the chemical order have been observed in particles with a diameter close to 2 nm [28, 33]. Both 2D-TEM grids and 3D-diluted samples have been prepared. The 3D samples used in magnetometry and EXAFS measurements have a concentration of only 0.5 % vol. in order to avoid coalescence and to keep the magnetic interactions negligible. Copper grids coated by a thin amorphous-carbon layer for TEM and high resolution transmission electron microscopy (HRTEM) observations, and silicon substrates for magnetic measurements have been used.

### Size distribution

The probability density function (PDF) of the diameter of mass selected clusters follows a Gaussian distribution[34, 35]. In the present case, PDFs of the incident CoPt and FePt clusters have been deduced from TEM observations. The NPs mean diameter are $D_{CoPt} = 3.2$ nm and $D_{FePt} = 3.4$ nm with a relative standard deviation $\sigma_D/D = 0.08$ for both CoPt and FePt NPs. Let us remind the reader that as-prepared nanoparticles are in the A1 chemically disordered phase [28]. To promote the chemically $L1_0$ ordered phase the samples have to be annealed at 600 °C during two hours.

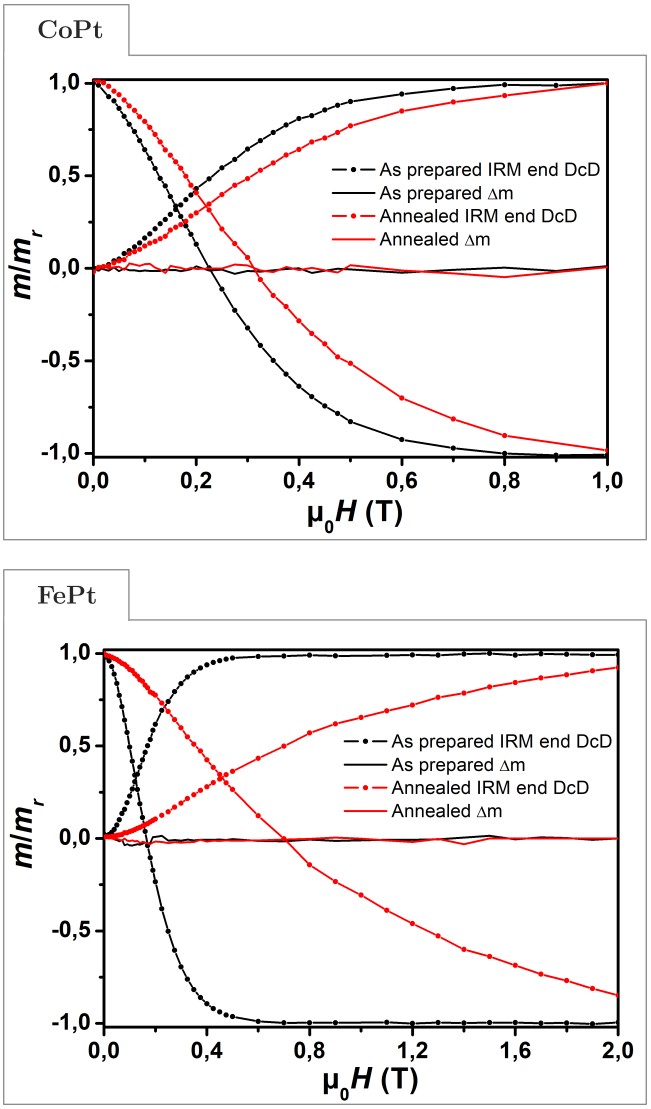


FIG. 1. IRM($H$), DcD($H$) and $\Delta m$ performed at $T = 2$ K of the CoPt and FePt samples before and after annealing.

### Magnetic interactions

All magnetic measurements have been performed in a commercial superconducting quantum interference device (SQUID) magnetometer (Quantum Design MPMS 5XL) at various temperatures. Isothermal remanent

magnetization (IRM) together with direct-current demagnetization (DcD) curves at low temperature have been used to detect the magnetic interactions between nanoparticles[36, 37].

In the IRM($H$) measurement the NP assembly is demagnetized by zero field cooling from the superparamagnetic regime. Then, a magnetic field $H$ is applied and removed: We acquire the isothermal remanent magnetic moment. By successively increasing $H$ and remove it, we finally obtain a full IRM($H$) curve. The maximum of the IRM($H$) curve is the remanent magnetic moment $m_R$ also measured in the hysteresis loop. In the DcD($H$) measurement the process is exactly the same, the only difference comes from the initial state which is $m_R$ (the maximum of the IRM($H$)). These two kinds of measurements, where the only difference is then the initial magnetic configuration, probe the irreversible magnetization switching [38], it means that there is no effect of superparamagnetic particles, diamagnetic substrate or paramagnetic impurities for instance. Moreover the IRM($H$) and DcD($H$) are also used to characterize the nature of interactions *via* the well known parameter $\Delta m$ = DcD($H$) - [$m_R$ - 2 IRM($H$)]. This parameter should be close to zero when interparticle interraction are negligible [36, 37, 39–41]. The IRM, DcD and $\Delta m$ curves for CoPt and FePt NP assemblies are given in fig. 1 before and after annealing. There is no detectable magnetizing ($\Delta m > 0$) or demagnetizing ($\Delta m < 0$) interactions in as-prepared and annealed nanomagnets, showing that clusters remain well separated inside the matrix even after annealing.

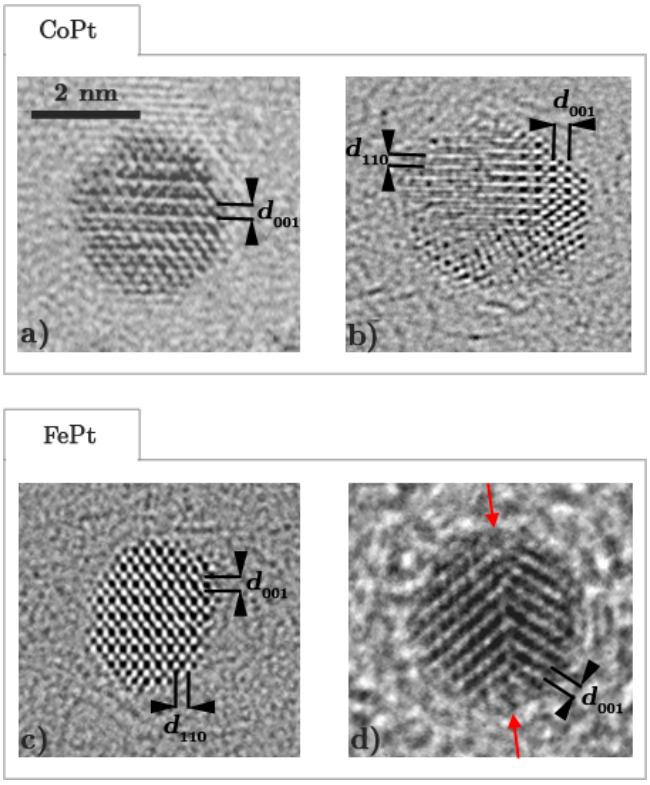


FIG. 2. HRTEM images of $L1_0$ (a) mono-domain and (b) multi-domain CoPt particles. HRTEM images of $L1_0$ (c) mono-domain FePt particle and (d) FePt particle exhibiting two $L1_0$ domains joined by a (111) twin. Note that the (001) and (110) periodicity are the signatures of $L1_0$ chemical order.

## III. CHEMICAL ORDERING

The samples are characterized by TEM in a high resolution mode (HRTEM). In addition to a JEOL 2010F microscope (operating at 200 kV and with a field emission gun), we have used a FEI Titan 80–300 microscope operating at 300 kV with a field emission gun and a Cs corrector for the objective lens. This yields HRTEM images with highly improved spatial resolution [42]. Both for annealed FePt and CoPt, we observe NPs with a single chemically ordered domain all along the nanoparticle (see fig. 2 (a) and (c)).

These monodomain NPs will be refered to as "$mono-L1_0$" particles in the following sections. The chemical order parameter ($S$) of "$mono-L1_0$" CoPt particles, with a diameter close to 3 nm, has been previously evaluated by HRTEM and simulations ($S \in [0.85, 1]$)[43].

We also observe chemical order in particles consisting of more than one crystalline domain. As an example we can observe in fig. 2 (b) a CoPt nanoparticle where the $L1_0$ order is clearly visible on top with a $L1_0$ domain (where $d_{001}$ is shown) which is not extending to the entire particle. However the zone where $d_{110}$ is shown is also chemically ordered but along a different direction.

(111) twins as displayed in fig. 2 (d) can lead to the observation of different orientations of $L1_0$ chemical order. We also observe decahedral particles, made of five $L1_0$ domains joined by (111) twin, and even icosahedral particles. Several theoretical investigations have predicted, for NPs smaller than 3 nm, the stability of these exotic structures displaying at the same time a fivefold symmetry and a chemical order [44–46].

All these particles, which are chemically ordered but with two or more $L1_0$ domain orientations, will be refereed to as "$multi-L1_0$" in the following sections. More informations about the chemical ordering of such nanoparticles can be found in [33].

The statistical abundance of each type of structure cannot be determined precisely using HRTEM[33]. Nevertheless, we are able to observe $mono-L1_0$ particles in both CoPt and FePt nanoalloys. From a magnetic point of view, it is expected that the uniaxial magnetic anisotropy of multi domain decahedral, icosahedral or twinned particles, despite the fact that they are all composed of ordered domains, will be lower than the uniaxial magnetic anisotropy of $mono-L1_0$ domain particles. In fact, locally, the orientation of the easy and hard axes

within each domain should be different. We can then anticipate at least two different magnetic behaviours in such samples composed of chemically ordered nanoparticles, the first one due to the $mono-L1_0$ NPs and the second one due to the $multi-L1_0$ NPs. In addition, we expect a significant anisotropy constant dispersion reflecting the variety of atomic arrangements in NPs[29].

## IV. MAGNETIC PROPERTIES

The high temperature ($T = 300$ K) and low temperature ($T = 2$ K) magnetization loops, ZFC/FC susceptibility curves, as well as the IRM (2 K) curve are shown in fig. 3 for CoPt and FePt clusters before and after annealing. All the ZFC/FC curves display the characteristic behaviour of an assembly of magnetic nanoparticles, namely a crossover between the blocked regime and the superparamagnetic regime.

At first glance, and for the as prepared samples (fig. 3 (a) and (c)) all the magnetic curves appear very similar for CoPt and FePt NPs. The magnetic characteristics of these fcc A1 clusters [28] seem to be almost the same, irrespective of chemical composition. After chemical ordering, the magnetic properties of CoPt NPs display a moderate change (fig. 3 (b) to compare to (a)). In particular the temperature corresponding to the maximum of the ZFC curves increases, as already observed in CoPt NPs with a larger size dispersion [28]. In contrast, for FePt clusters, the magnetic behaviour drastically changes upon annealing (see fig. 3 (c) and (d), note that the axis scales are different). The shape of the ZFC/FC curves (fig. 3 (d)) indicates the presence of a large distribution of magnetic anisotropy energies as the splitting temperature between ZFC and FC is very high (180 K) compared to the maximum of the ZFC ($T_{\max} = 60$ K).

A more quantitative analysis is possible thanks to a previously developed theoretical framework enabling a global fitting procedure of the entire set of magnetic measurements [47–50]. In this way the magnetic measurements can be reproduced with a limited number of parameters which describe the nanomagnets regarded as non-interacting macrospins. These are the magnetic size distribution (Gaussian with an average diameter $D$ and a standard deviation $\sigma$), the first order anisotropy constant distribution (assumed to be Gaussian [49] with an average anisotropy constant $\overline{K_1}$ and a standard deviation $\sigma_{K_1}$) and the biaxial anisotropy ratio $K_2/K_1$. Such biaxial description is used to reflect the non ideal morphology of the nanoparticles [48, 51]. The actual global fits are presented in figure 3 for each sample by the red solid curves. The corresponding fitting parameters are summarized in Table I.

The chemically disordered CoPt and FePt A1 NPs exhibit identical magnetic properties within the experimental uncertainty. The mean anisotropy constant $\overline{K_1}$ and the $K_2/K_1$ ratio are almost the same as those measured in pure fcc Co NPs [52]. In fact, both CoPt and FePt A1 NPs behave similarly as fcc Co particles, where the biaxial contribution and the value of $K_1$ can be explained by the presence of additional or incomplete facets at the surface of the particles [50, 53–55]. This shows that before annealing the magnetic anisotropy of the chemically disordered particles is dominated by the shape and the surface structure.

Let us remind the reader that after annealing HRTEM study has previously shown monodomain $L1_0$ ($mono-L1_0$) NPs and multidomain $L1_0$ ($multi-L1_0$) NPs in both CoPt and FePt alloys.

First we will discuss the magnetic properties of FePt NPs after annealing and then the annealed CoPt NPs. For the annealed FePt NPs we use a bimodal anisotropy constant distribution in order to reproduce accurately the experimental curves (table I and figure 4 where two peaks are presents). If we use only one large anisotropy constant distribution (gaussian or log-normal) some important points of the curves (merging point between the ZFC and FC, or narrowing of the hysteresis loop at $m = 0$) are not reproduced. The simplest distribution which allows to perform a satisfactory fit is a bimodal gaussian anisotropy constant distribution.

Motivated by the HRTEM observations of both monodomain ($mono-L1_0$) and multidomain ($multi-L1_0$) FePt NPs, we consider that each of these types of structure should have its own anisotropy constant distribution. Then, the mean anisotropy constant of the $multi-L1_0$ FePt NPs is around 400 kJ.m$^{-3}$, whereas $mono-L1_0$ FePt NPs exhibit a strong mean anisotropy constant around 1.1 MJ.m$^{-3}$.

Note that 30 % of the FePt NPs exhibit an anisotropy constant ($K_1$) higher than 1 MJ.m$^{-3}$ and the switching field of some $L1_0$ FePt clusters is higher than 2 T (fig. 3 (d)). In addition, the $K_2/K_1$ ratio is lower for the FePt $mono-L1_0$ NPs ($K_2/K_1 = 0.3$) . This feature suggests that, for the FePt $mono-L1_0$ NPs, the principal contribution to the magnetic anisotropy energy comes from the $L1_0$ stacking (shape and faceting lead to a biaxial anisotropy[50, 51, 53, 54])).

After annealing, the CoPt magnetic anisotropy slightly increases [28], which is visible as $T_{max}$ and $\mu_0 H_c$ enhancements (fig.3). This feature is attributed to the chemical ordering. The $K_2/K_1$ ratio is almost the same (table I), which suggests that the magnetic anisotropy still reflects the surface contributions. However, the most important difference between annealed CoPt and FePt NPs is that only one Gaussian anisotropy constant distribution is necessary in order to reproduce all the magnetic measurements performed on the annealed CoPt NPs (see figure 4). These features indicate that magnetic anisotropy constants of $mono-L1_0$ and $multi-L1_0$ CoPt clusters are similar. In all the magnetic measurements there is no sign of a high magnetic anisotropy in chemically ordered

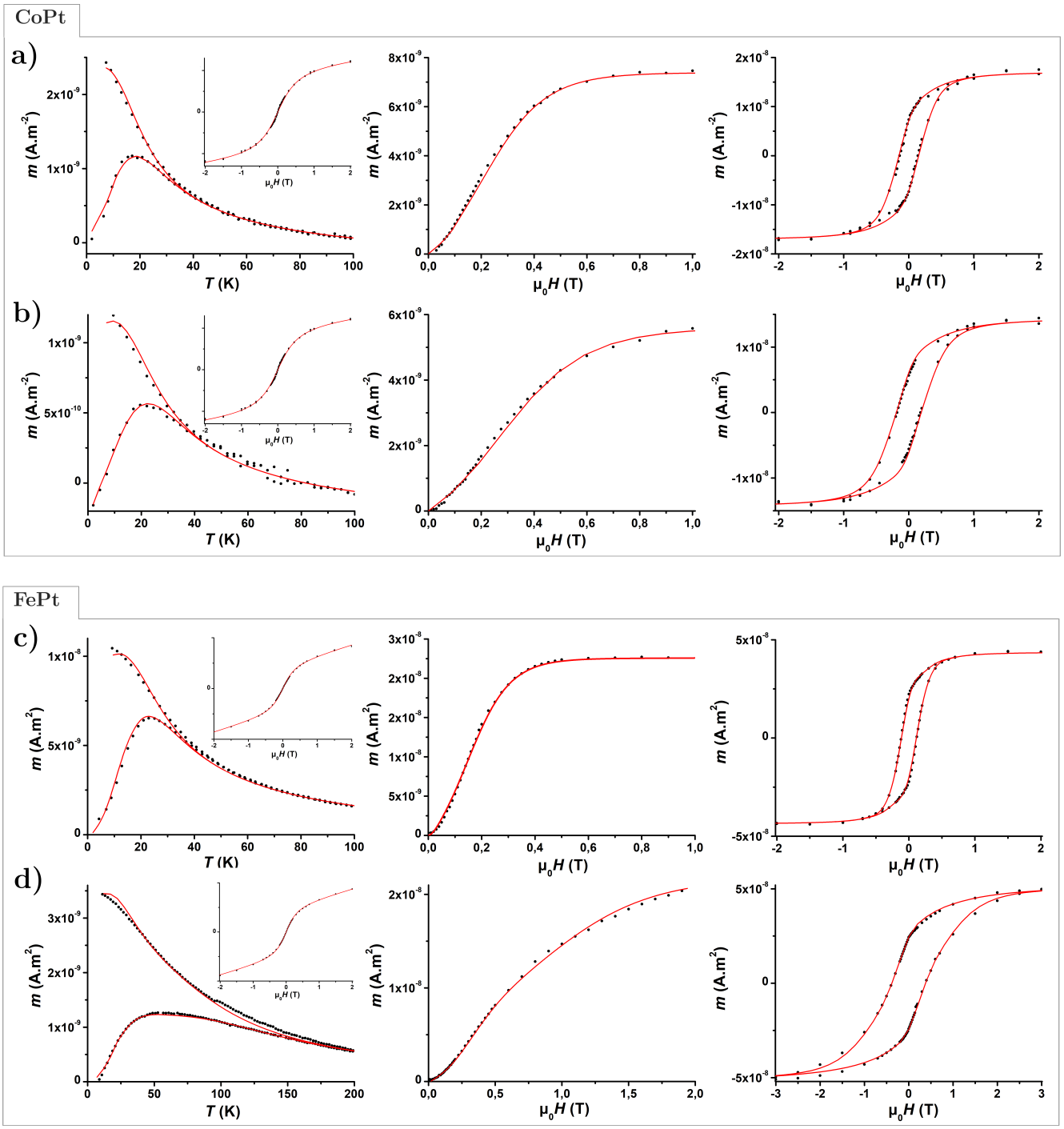


FIG. 3. Experimental (black dots) and simulated (red solid lines) ZFC/FC curves, superparamagnetic magnetization loop at 300 K (in inset), IRM curve and hysteresis loop at 2 K, for CoPt (a,b) and FePt (c,d) clusters before annealing (a,c) and after annealing (b, d). Taking into account a second order anisotropy term $K_2$ and a distribution of anisotropy constant $K_1$ is necessary in order to accurately simulate all the curves. Note that the horizontal scales are different for annealed FePt clusters (d).

CoPt NPs.

As already mentioned, in bulk material the anisotropy constant is 5 and 7 MJ.m$^{-3}$ [17] (and references therein) respectively for CoPt and FePt $L1_0$ alloys. Even for the $mono - L1_0$ FePt NPs, the magnetic anisotropy ($K_1$ = 1.1 MJ.m$^{-3}$) is reduced compared to the bulk. Some theoretical studies, performed on perfect CoPt and FePt $L1_0$ nanoparticles, have shown that for small sizes the magnetic anisotropy constant should slightly decrease [56–58]. In fact, cluster surface breaks the $L1_0$ period-

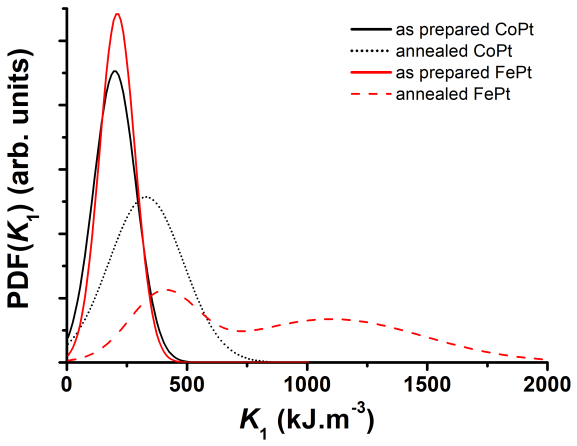


FIG. 4. Magnetic anisotropy distribution of the A1 and $L1_0$ particles, as deduced from magnetic measurement fits.

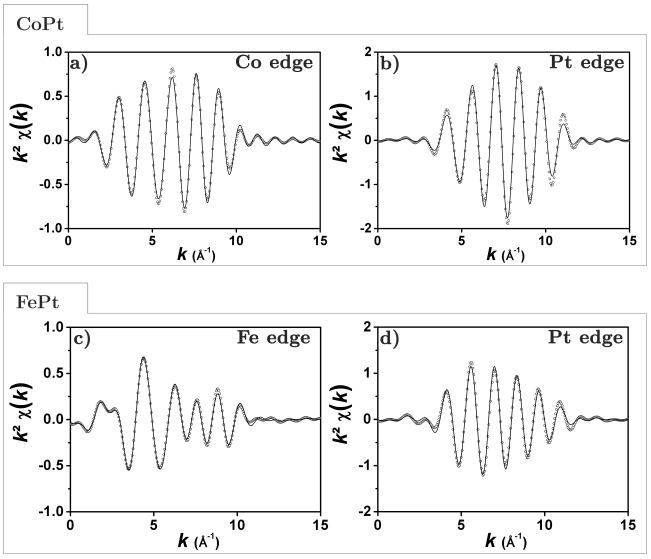


FIG. 5. Comparison between the experimental EXAFS signal (dots, contribution of the nearest neighbours (NN) peak only) and simulated curves (solid lines) at the Co-K edge a), Fe-K edge c) and at the Pt-L edge b) and d) obtained on the chemically ordered CoPt and FePt particles.

icity which implies a decrease of the uniaxial magnetic anisotropy.

Finally the determination of the magnetic properties leads to a major question: Why is the magnetic anisotropy magnitude comparable in $multi - L1_0$ and $mono - L1_0$ CoPt NPs whereas it is possible to distinguish two different magnetic behaviours in FePt?

## IV. ATOMIC FINE STRUCTURE

In order to answer these questions, we have performed extended X-ray absorption fine structure (EXAFS) measurements on the annealed CoPt and FePt particles. XAS at the Co-K, Fe-K and Pt-L edges have been performed at room temperature on the CRG BM30b-FAME [59] and ID12 beamlines [60] of the ESRF. A quantitative EXAFS analysis is performed by fitting the $k^2$-weighted function $\chi(k)$ to the standard EXAFS formula, using the Artemis software [61] and focusing on the nearest neighbours (NN) contribution. Debye-Waller (DW) parameters are used to account for bond-length dispersion. The edge energy is allowed to slightly vary for the different samples but is taken to be the same for the Pt, Co and Fe neighboring shells. The experimental and adjusted curves are presented figure 5 and the best fits values are summarized in table II.

A transition metal (TM) atom is surrounded by $N_{\mathrm{TM}}$ atoms at a distance $d_{\mathrm{TMTM}}$ and $N_{\mathrm{Pt}}$ platinum atoms at a distance $d_{\mathrm{TMPt}}$. As expected from the HRTEM observations, the ratios $N_{\mathrm{Pt}}/N_{\mathrm{TM}} = 2$ at the TM edges and $N_{\mathrm{TM}}/N_{\mathrm{Pt}} = 2$ at the Pt edges, corresponding to chemically ordered NPs, allow us to adjust quasi-perfectly the experimental measurements (figure 5). This results corroborates, on the NPs assemblies, the observations performed in HRTEM.

Interestingly, the deduced from fits DW parameter is unusually large ($\approx 10^{-2}$Å$^2$ mean square relative displacement) for the TM-TM, TM-Pt and Pt-Pt bonds which is the signature of a significant dispersion of NN distances [62].

As shown in table II, the TMPt distances are different from the $d_{\mathrm{TMTM}}$ and $d_{\mathrm{PtPt}}$, which are themselves different, contrary to the bulk crystal (where $d_{\mathrm{TMTM}}$ and $d_{\mathrm{PtPt}}$ are equal). Then two apparent $c/a$ tetragonalization ratios can be inferred from these distances, assuming a face-centered tetragonal (fct) crystal structure: $(c/a)_{TM} = \sqrt{2(d_{\mathrm{TMPt}}/d_{\mathrm{TMTM}})^2 - 1}$ and $(c/a)_{Pt} = \sqrt{2(d_{\mathrm{TMPt}}/d_{\mathrm{PtPt}})^2 - 1}$. $(c/a)_{TM}$ can thus be evaluated from distances around the TM atoms, while $(c/a)_{Pt}$ is calculated from distances around the Pt atoms (see table II). In the bulk crystal, both approaches are the same, but in NPs, the values inferred from EXAFS measurements reflect the local environment around a given type of atom. The fact that there are two different apparent $c/a$ means that the perfect crystalline structure is perturbed [63, 64].

Strikingly, the Co environment corresponds to an apparent tetragonilization opposite to the bulk ($c/a > 1$, remember that the $c/a$ ratio in the bulk $L1_0$ CoPt and FePt are almost similar and approximatively equal to 0.97 [65]). For FePt we also find a larger apparent $c/a$ around Fe atoms ($c/a \simeq 1$) even if the difference between the values deduced from both absorption edges is smaller than in CoPt NPs. This shows that the atomic relaxation is more pronounced in CoPt than in FePt NPs: In

| Sample | $T_{max}$(K) | $\mu_0 H_c$(mT) | $D$(nm) | $\sigma/D$ | $\overline{K}_1$(kJ/m$^3$) | $\sigma_{K_1}/\overline{K}_1$ | $K_2/K_1$ |
|---|---|---|---|---|---|---|---|
| As-prepared CoPt | 19 | 0.13 | $3.2 \pm 0.2$ | $0.10 \pm 0.02$ | $200 \pm 20$ | $0.44 \pm 0.15$ | $1.2 \pm 0.2$ |
| Annealed CoPt | 22 | 0.18 | $3.2 \pm 0.2$ | $0.10 \pm 0.02$ | $330 \pm 30$ | $0.47 \pm 0.15$ | $1.2 \pm 0.2$ |
| As-prepared FePt | 22 | 0.12 | $3.5 \pm 0.2$ | $0.10 \pm 0.02$ | $210 \pm 20$ | $0.32 \pm 0.15$ | $1.0 \pm 0.2$ |
| Annealed FePt | 55 | 0.37 | $3.5 \pm 0.2$ | $0.10 \pm 0.02$ | $400 \pm 40$ | $0.35 \pm 0.15$ | $1.0 \pm 0.2$ |
| | | | | | $1100 \pm 150$ | $0.35 \pm 0.15$ | $0.3 \pm 0.2$ |

TABLE I. For each sample, ZFC peak temperature ($T_{max}$), low temperature coercivity ($\mu_0 H_c$), median magnetic diameter ($D$) and dispersion parameter ($\sigma$) of the Gaussian particle size distribution, median anisotropy constant ($K_1$) and standard deviation ($\sigma_{K_1}$) of the anisotropy constant distribution, and biaxial anisotropy ratio $K_2/K_1$ determined by a global fit of the ZFC/FC suscpetibility curves, low temperature IRM curve and $m(H)$ loops at 2 K and 300 K. The clusters magnetizations have been deduced from XMCD measurements [31], *i.e.* $10^6$ and $1.28.10^6$ A.m$^{-1}$, respectively for CoPt and FePt clusters.

other words, the atomic structure of small FePt clusters is closer to a bulk $L1_0$ crystal than for CoPt clusters. Let us emphasize that EXAFS measurements only probe the local environment and, despite they bear the signature of chemical $L1_0$ order, they cannot discriminate between $mono-L1_0$ and $multi-L1_0$ NPs.

The different relaxation magnitude in CoPt and FePt NPs suggests that the different magnetic anisotropy properties identified in section III could result from a local modification of the tetragonilazation ($c/a$ ratio). Some theoretical bulk calculations have already correlated the $c/a$ ratio, the degree of chemical order and the magnetic anisotropy energy [66–69]. It has been shown that a modification of the $c/a$ ratio in a range as the one deduced from EXAFS (see table II) only has a weak influence on the magnetic anisotropy.

We can then argue that the different local tetragonalization in CoPt versus FePt NPs does not seem to be the reason of the different magnetic behaviour in both nanoalloys. In order to get a deeper understanding of the relaxation effects, we have performed first-principles calculations.

| Sample | | $d_{\mathrm{TMTM}}$ (nm) | $d_{\mathrm{TMPt}}$ (nm) | $d_{\mathrm{PtPt}}$ (nm) | $c/a$ |
|---|---|---|---|---|---|
| CoPt | Co edge | 0.257 | 0.262 | | 1.04±0.02 |
| | Pt edge | | 0.262 | 0.271 | 0.93±0.02 |
| FePt | Fe edge | 0.263 | 0.263 | | 1.00±0.02 |
| | Pt edge 0.272 | | 0.263 | 0.270 | 0.95±0.02 |

TABLE II. For each annealed sample, distances between nearest neighbours deduced from the EXAFS fits and apparent $c/a$ ratios (see text).

## V. STRUCTURAL RELAXATION CALCULATIONS

The calculations have been performed by using the Vienna *ab initio* simulation package [70, 71] which implements Hohenberg-Kohn-Sham's density-functional theory (DFT) on a periodic supercell and allows fully self-consistent unconstrained structural relaxations. It should be however noted that our goal cannot be to explain or reproduce the experimental EXAFS results in their full extent. In fact the EXAFS experiment is performed on a very large variety of chemically ordered nanoparticles (monodomain, multidomain, icosahedral, ...(see section II)) and therefore reflect only a mean value of the apparent tetragonalization which can be different for individual structure.

| Sample | | $d_{\mathrm{TMTM}}$ (nm) | $d_{\mathrm{TMPt}}$ (nm) | $d_{\mathrm{PtPt}}$ (nm) | $c/a$ |
|---|---|---|---|---|---|
| CoPt | Co sites | 0.264 | 0.264 | | 1.00 |
| | Pt sites | | 0.264 | 0.270 | 0.95 |
| FePt | Fe sites | 0.270 | 0.267 | | 0.98 |
| | Pt sites | | 0.267 | 0.273 | 0.96 |

TABLE III. Average interatomic distances and "apparent" $c/a$ ratios (see text) for relaxed $L1_0$ CoPt and FePt clusters having 586 atoms, as obtained from DFT calculations.

We have then performed a first-principles theoretical study of the structure of monodomain $L1_0$ CoPt and FePt particles. The assumed particle geometries are perfect truncated octahedra having 38, 201 and 586 atoms. The truncated octahedron is a equilibrium shape predicted by Wulff theory and even if the actual structure of some particles may be different, we expect that the atomic relaxation mechanism are robust enough to give insight both for $mono-L1_0$ and $multi-L1_0$ NPs. Moreover the most intriguing magnetic feature concerns $mono-L1_0$ particles (which for CoPt, seems to have a much lower anisotropy than for the bulk).

Table III compares the mean interatomic distance in chemically $L1_0$ ordered CoPt and FePt truncated octahedron with 586 atoms. The mean TM nearest neighbour bonds is shorter than the Pt ones leading to a structural stress, and we find that a finite TMPt cluster can be more easily distorted by moving the TM atoms. This effect is particularly strong in the CoPt alloy (see figure 6).

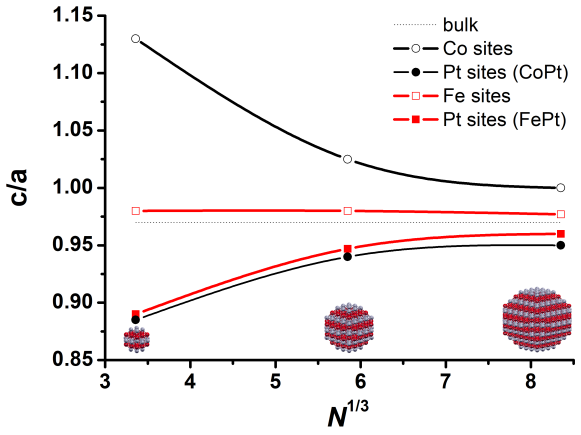


FIG. 6. Comparison between the "apparent" $c/a$ ratios for the MT and Pt sites. $N$ represents the number of atoms used to build perfect truncated octahedrons ($N^{1/3}$ periodicity). The lines are drawn to guide the eye. The dashed line represents the $c/a$ ratio in the $L1_0$ bulk phase.

Following the EXAFS analysis, we can compute an "apparent" $c/a$, which is here defined around the two types of atoms by using the average nearest neighbour TMPt and either PtPt or TMTM distances. This quantity is then a ratio of mean values, rather than a mean local tetragonalization.

The "apparent" $c/a$ ratios at the TM sites are obviously different in both alloys, whereas the "apparent" $c/a$ ratio at the Pt sites is almost the same. The relaxation effect is clearly less significant in FePt nanoparticles. This feature is in agreement with the conclusions deduced from experimental EXAFS results. The "apparent" $c/a$ ratio appears to be a simple tool in order to qualitatively compare EXAFS results and theoretical investigations but it does not reflect the full complexity associated with atomic relaxations in finite size clusters. In particular it would be too simplistic to conclude that the relaxation only induces a different local tetragonalization in FePt and CoPt NPs. What is striking, more than the deviation from the bulk value, is the large magnitude of the "apparent" $c/a$ difference between Co and Pt sites. This is the signature of a strong relaxation, especially for Co atoms which means a significant breaking of the $L1_0$ crystal symmetry.

To go further we plot in figure 7 all the NN's distance calculated for clusters having 586 atoms. It becomes clear then, even if the mean distances are close to the bulk values for both nanoalloys (see table III), that the distributions of the $d_{\mathrm{CoCo}}$ and $d_{\mathrm{FeFe}}$ are completely different. The standard deviation of $d_{\mathrm{CoCo}}$ is extremely large ($\sigma(d_{\mathrm{CoCo}}) = 0.017$ nm), whereas for FePt NPs the distribution of both $d_{\mathrm{FeFe}}$ and $d_{\mathrm{PtPt}}$ are narrow ($\sigma(d_{\mathrm{FeFe}}) = 0.004$ nm). In fact, this appears to be

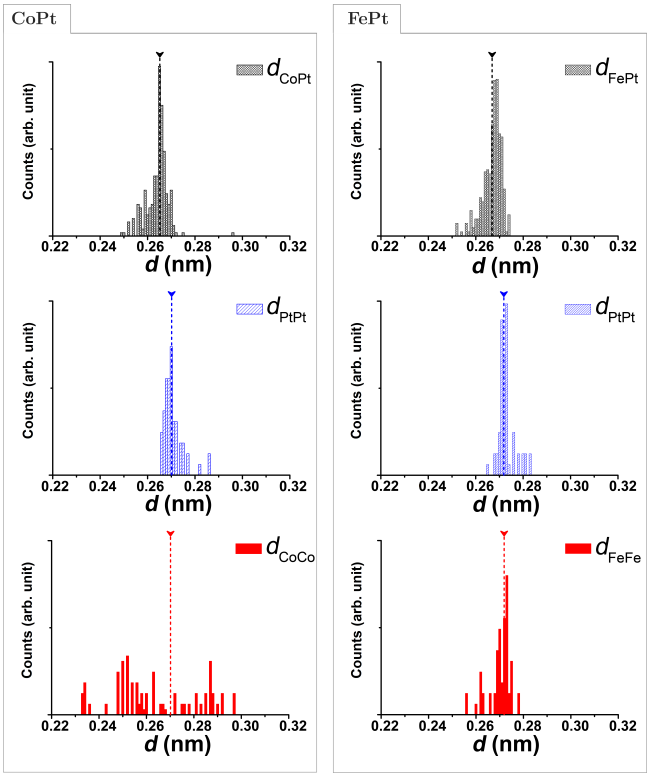


FIG. 7. NN's distances obtained from calculations on chemically ordered CoPt and FePt nanoparticles (586 atoms) . The arrows represent distances in the $L1_0$ bulk alloys. To facilitate a clear comparison, the used scales are identical.

the major structural difference between both nanoalloys. Although the particles are chemically ordered, atomic relaxation induces an important crystallographic disorder, especially in the Co planes. The relaxed CoPt NPs structure is far from a perfect crystal [63]. Comparatively, we find that in FePt NPs the behavior of Fe atoms is comparable to Pt atoms, with a moderate disordering.

This striking difference between CoPt and FePt NPs should be reflected in their magnetic properties. We can then infer that the reduced magnetic anisotropy in CoPt, where even the presence of $mono - L1_0$ is not accompanied with a large anisotropy contribution, is due to the specific finite size relaxation and more precisely to the wide $d_{\mathrm{CoCo}}$ interatomic distance distribution. Following this idea, since the atomic relaxation is lower in $L1_0$ FePt NPs (narrower $d_{\mathrm{FeFe}}$ distribution ), it allows us to explain why the anisotropy of $mono - L1_0$ particles is so large (in the MJ.m$^{-3}$ range). Besides, it should be kept in my mind that for both FePt and CoPt, there are many different NP geometries, in particular there exist $multi - L1_0$ particles which give a wide anisotropy distribution centred around a similar value ($\overline{K_1} \simeq 350$ kJ.m$^{-3}$). Finally a complete and systematic theoretical study of the magnetic properties in these relaxed structure needs to be done in order to fully understand the de-

tailed mechanisms linking the atomic structure and the magnetic anisotropy. Such a numerical investigation is delicate and beyond the scope of the present article.

## VI. CONCLUSION

The structure and magnetic properties of both chemically ordered CoPt and FePt nanoparticles have been investigated. Although they are very similar for the bulk $L1_0$ phase, we find striking differences in terms of magnetic anisotropy. In particular, for FePt NPs a strong anisotropy contribution ($K_1 = 1.1$ MJ.m$^{-3}$) can be attributed to $mono-L1_0$ particles, whereas CoPt NPs exhibit a much reduced magnetic anisotropy ($K_1 = 330$ kJ.m$^{-3}$) even if $mono-L1_0$ particles are also observed. From an application point of view, if the goal is to obtain a strong anisotropy, a strong switching field and a high blocking temperature, then FePt appears to be preferable to CoPt.

EXAFS measurements have been used to determine the atomic structure of annealed CoPt and FePt NPs. We find that the NPs are chemically ordered, but with different apparent tetragonalization ratios. DFT calculations on relaxed $mono-L1_0$ truncated octahedral clusters shed light on the finite size atomic relaxation effects: The $L1_0$ crystalline order is disturbed, especially in CoPt NPs where we find a wide $d_{\mathrm{CoCo}}$ interatomic distance distribution. This feature, which is absent in the case of FePt NPs, could explain the major anisotropy difference between both nanoalloys. Additional finite size effects, namely the existence of numerous particle geometries with potential strain, defects, and surface disorder [72, 73], may play a role in the magnetic anisotropy reduction compared to the bulk, as well as in the difference between FePt and CoPt alloys. Further progress requires a systematic and profound theoretical investigation to relate the magnetic properties to the detailed atomic structure.

### Acknowledgments

This work has been funded through the "Plateforme LYonnaise de Recherche sur les Agrégats" (PLYRA) and the "Centre de Magnétométrie de Lyon" (CML). The authors would like to acknowledge support from CONACYT (Mexico) and International Research Network (IRN) Nanoalloys (CNRS).

* alexandre.tamion@univ-lyon1.fr

[1] Z. Fan, M. Shelton, A. K. Singh, D. Senapati, S. A. Khan, and P. C. Ray, ACS nano **6**, 1065 (2012).
[2] A. K. Gupta and M. Gupta, Biomaterials **26**, 3995 (2005).
[3] T. A. Larson, J. Bankson, J. Aaron, and K. Sokolov, Nanotechnology **18**, 325101 (2007).
[4] W.-R. Lee, M. G. Kim, J.-R. Choi, J.-I. Park, S. J. Ko, S. J. Oh, and J. Cheon, Journal of the American Chemical Society **127**, 16090 (2005).
[5] A.-H. Lu, E. L. Salabas, and F. Schüth, Angewandte Chemie International Edition **46**, 1222 (2007).
[6] D. M. Newman, M. L. Wears, M. Jollie, and D. Choo, Nanotechnology **18**, 205301 (2007).
[7] R. Sharma and C. J. Chen, Journal of Nanoparticle Research **11**, 671 (2008).
[8] M. Shliomis and V. Stepanov, Journal of Magnetism and Magnetic Materials **122**, 176 (1993).
[9] S. U. Son, Y. Jang, J. Park, H. B. Na, H. M. Park, H. J. Yun, J. Lee, and T. Hyeon, Journal of the American Chemical Society **126**, 5026 (2004).
[10] C. Xu, K. Xu, H. Gu, X. Zhong, Z. Guo, R. Zheng, X. Zhang, and B. Xu, Journal of the American Chemical Society **126**, 3392 (2004).
[11] S. Sun, Science **287**, 1989 (2000).
[12] Y. Chen, F. Yang, Y. Dai, W. Wang, and S. Chen, Journal of Physical Chemistry C **112**, 1645 (2008).
[13] D. L. Huber, Small (Weinheim an der Bergstrasse, Germany) **1**, 482 (2005).
[14] A. Tamion, M. Hillenkamp, A. Hillion, V. A. Maraloiu, I. D. Vlaicu, M. Stefan, D. Ghica, H. Rositi, F. Chauveau, M.-G. Blanchin, M. Wiart, and V. Dupuis, Nano Research **9**, 2398 (2016).
[15] E. Wohlfarth, Physics Letters A **70**, 489 (1979).
[16] P. Andreazza, V. Pierron-Bohnes, F. Tournus, C. Andreazza-Vignolle, and V. Dupuis, Surface Science Reports **70**, 188 (2015).
[17] K. Barmak, J. Kim, L. H. Lewis, K. R. Coffey, M. F. Toney, A. J. Kellock, and J.-U. Thiele, Journal of Applied Physics **98**, 033904 (2005).
[18] A. C. C. Yu, M. Mizuno, Y. Sasaki, M. Inoue, H. Kondo, I. Ohta, D. Djayaprawira, and M. Takahashi, Applied Physics Letters **82**, 4352 (2003).
[19] M. Yu, Y. Liu, and D. J. Sellmyer, Journal of Applied Physics **87**, 6959 (2000).
[20] Y. Xu, Z. Sun, Y. Qiang, and D. Sellmyer, Journal of Magnetism and Magnetic Materials **266**, 164 (2003).
[21] M. S. Wellons, Z. Gai, J. Shen, J. Bentley, J. E. Wittig, and C. M. Lukehart, Journal of Materials Chemistry C **1**, 5976 (2013).
[22] T. Seto, K. Koga, H. Akinaga, F. Takano, T. Orii, and M. Hirasawa, Journal of Nanoparticle Research **8**, 371 (2006).
[23] J. H. Kim, J. Kim, N. Oh, Y.-H. Kim, C. K. Kim, C. S. Yoon, and S. Jin, Applied Physics Letters **90**, 023117 (2007).
[24] C. N. Chinnasamy, B. Jeyadevan, K. Shinoda, and K. Tohji, Journal of Applied Physics **93**, 7583 (2003).
[25] D. Alloyeau, C. Langlois, C. Ricolleau, Y. Le Bouar, and A. Loiseau, Nanotechnology **18**, 375301 (2007).
[26] M. Pellarin, E. Cottancin, J. Lermé, J. L. Vialle, J. P. Wolf, M. Broyer, V. Paillard, V. Dupuis, A. Perez, and J. P. Perez, Chemical physics letters **224**, 338 (1994).
[27] A. Perez, P. Melinon, V. Dupuis, L. Bardotti, B. Masenelli, F. Tournus, B. Prevel, J. Tuaillon-Combes, E. Bernstein, and A. Tamion, International Journal of Nanotechnology **7**, 523 (2010).

[28] F. Tournus, A. Tamion, N. Blanc, A. Hannour, L. Bardotti, B. Prével, P. Ohresser, E. Bonet, T. Epicier, and V. Dupuis, Physical Review B **77** (2008), 10.1103/PhysRevB.77.144411.

[29] F. Tournus, N. Blanc, A. Tamion, M. Hillenkamp, and V. Dupuis, Physical Review B **81** (2010), 10.1103/PhysRevB.81.220405.

[30] A. Hillion, A. Cavallin, S. Vlaic, A. Tamion, F. Tournus, G. Khadra, J. Dreiser, C. Piamonteze, F. Nolting, S. Rusponi, K. Sato, T. J. Konno, O. Proux, V. Dupuis, and H. Brune, Physical Review Letters **110** (2013), 10.1103/PhysRevLett.110.087207.

[31] V. Dupuis, G. Khadra, S. Linas, A. Hillion, L. Gragnaniello, A. Tamion, J. Tuaillon-Combes, L. Bardotti, F. Tournus, E. Otero, P. Ohresser, A. Rogalev, and F. Wilhelm, Journal of Magnetism and Magnetic Materials **383**, 73 (2015).

[32] C.-b. Rong, D. Li, V. Nandwana, N. Poudyal, Y. Ding, Z. L. Wang, H. Zeng, and J. P. Liu, Advanced Materials **18**, 2984 (2006).

[33] F. Tournus, K. Sato, T. Epicier, T. J. Konno, and V. Dupuis, Physical Review Letters **110** (2013), 10.1103/PhysRevLett.110.055501.

[34] R. Alayan, L. Arnaud, A. Bourgey, M. Broyer, E. Cottancin, J. R. Huntzinger, J. Lermé, J. L. Vialle, M. Pellarin, and G. Guiraud, Review of Scientific Instruments **75**, 2461 (2004).

[35] D. Tainoff, L. Bardotti, F. Tournus, G. Guiraud, O. Boisron, and P. Mélinon, The Journal of Physical Chemistry C **112**, 6842 (2008).

[36] E. P. Wohlfarth, Journal of Applied Physics **29**, 595 (1958).

[37] O. Henkel, physica status solidi (b) **7**, 919 (1964).

[38] F. Tournus, Journal of Magnetism and Magnetic Materials **375**, 194 (2015).

[39] F. Wehland, A. Stancu, P. Rochette, M. Dekkers, and E. Appel, Physics of the Earth and Planetary Interiors **153**, 181 (2005).

[40] J. M. Martínez Huerta, J. De La Torre Medina, L. Piraux, and A. Encinas, Journal of Applied Physics **111**, 083914 (2012).

[41] A. Hillion, A. Tamion, F. Tournus, C. Albin, and V. Dupuis, Physical Review B **95** (2017), 10.1103/PhysRevB.95.134446.

[42] K. Sato, T. J. Konno, and Y. Hirotsu, J. Appl. Phys. **105**, 034308 (2009).

[43] N. Blanc, F. Tournus, V. Dupuis, and T. Epicier, Physical Review B **83**, 092403 (2011).

[44] P. Entel, M. Gruner, G. Rollmann, A. Hucht, S. Sahoo, A. Zayak, H. Herper, and A. Dannenberg, Philosophical Magazine **88**, 2725 (2008).

[45] G. Rossi, R. Ferrando, and C. Mottet, Faraday Discuss. **138**, 193 (2008).

[46] P. Andreazza, C. Mottet, C. Andreazza-Vignolle, J. Penuelas, H. C. N. Tolentino, M. De Santis, R. Felici, and N. Bouet, Physical Review B **82**, 155453 (2010).

[47] A. Tamion, M. Hillenkamp, F. Tournus, E. Bonet, and V. Dupuis, Applied Physics Letters **95**, 062503 (2009).

[48] A. Tamion, E. Bonet, F. Tournus, C. Raufast, A. Hillion, O. Gaier, and V. Dupuis, Physical Review B **85** (2012), 10.1103/PhysRevB.85.134430.

[49] A. Hillion, A. Tamion, F. Tournus, O. Gaier, E. Bonet, C. Albin, and V. Dupuis, Physical Review B **88** (2013), 10.1103/PhysRevB.88.094419.

[50] S. Oyarzún, A. Tamion, F. Tournus, V. Dupuis, and M. Hillenkamp, Scientific Reports **5** (2015), 10.1038/srep14749.

[51] A. Thiaville, Physical Review B **61**, 12221 (2000).

[52] A. Tamion, C. Raufast, M. Hillenkamp, E. Bonet, J. Jouanguy, B. Canut, E. Bernstein, O. Boisron, W. Wernsdorfer, and V. Dupuis, Physical Review B **81** (2010), 10.1103/PhysRevB.81.144403.

[53] M. Jamet, W. Wernsdorfer, C. Thirion, D. Mailly, V. Dupuis, P. Mélinon, and A. Pérez, Physical Review Letters **86**, 4676 (2001).

[54] M. Jamet, W. Wernsdorfer, C. Thirion, V. Dupuis, P. Mélinon, A. Pérez, and D. Mailly, Physical Review B **69** (2004), 10.1103/PhysRevB.69.024401.

[55] Y. Xie and J. A. Blackman, Journal of Physics: Condensed Matter **16**, 3163 (2004).

[56] S. Rohart, F. Tournus, and V. Dupuis, arXiv:1105.6292 [cond-mat] (2011), arXiv: 1105.6292.

[57] Z. Liu and G. Wang, Physical Review B **96** (2017), 10.1103/PhysRevB.96.224412.

[58] R. Cuadrado and R. W. Chantrell, Physical Review B **86** (2012), 10.1103/PhysRevB.86.224415.

[59] O. Proux, V. Nassif, A. Prat, O. Ulrich, E. Lahera, X. Biquard, J.-J. Menthonnex, and J.-L. Hazemann, Journal of Synchrotron Radiation **13**, 59 (2006).

[60] J. Goulon, A. Rogalev, G. Goujon, C. Gauthier, E. Moguiline, A. Solé, S. Feite, F. Wilhelm, N. Jaouen, C. Goulon-Ginet, P. Dressler, P. Rohr, M.-O. Lampert, and R. Henck, Journal of Synchrotron Radiation **12**, 57 (2005).

[61] B. Ravel and M. Newville, Journal of Synchrotron Radiation **12**, 537 (2005).

[62] G. Greco, A. Witkowska, E. Principi, M. Minicucci, and A. Di Cicco, Physical Review B **83** (2011), 10.1103/PhysRevB.83.134103.

[63] N. Blanc, L. E. Díaz-Sánchez, A. Y. Ramos, F. Tournus, H. C. N. Tolentino, M. De Santis, O. Proux, A. Tamion, J. Tuaillon-Combes, L. Bardotti, O. Boisron, G. M. Pastor, and V. Dupuis, Physical Review B **87** (2013), 10.1103/PhysRevB.87.155412.

[64] M. Hennes, E. Fonda, N. Casaretto, J. Buchwald, X. Weng, G. Patriarche, D. Demaille, Y. Zheng, and F. Vidal, Physical Review Materials **4**, 126001 (2020).

[65] A. Menshikov, T. Tarnóczi, and E. Krén, physica status solidi (a) **28**, K85 (1975).

[66] J. B. Staunton, S. Ostanin, S. S. A. Razee, B. Gyorffy, L. Szunyogh, B. Ginatempo, and E. Bruno, Journal of Physics: Condensed Matter **16**, S5623 (2004).

[67] T. Burkert, O. Eriksson, S. I. Simak, A. V. Ruban, B. Sanyal, L. Nordström, and J. M. Wills, Physical Review B **71** (2005), 10.1103/PhysRevB.71.134411.

[68] P. V. Lukashev, N. Horrell, and R. F. Sabirianov, Journal of Applied Physics **111**, 07A318 (2012).

[69] Y. Yang, C.-C. Chen, M. C. Scott, C. Ophus, R. Xu, A. Pryor, L. Wu, F. Sun, W. Theis, J. Zhou, M. Eisenbach, P. R. C. Kent, R. F. Sabirianov, H. Zeng, P. Ercius, and J. Miao, Nature **542**, 75 (2017).

[70] G. Kresse and J. Furthmüller, Physical Review B **54**, 11169 (1996).

[71] G. Kresse and D. Joubert, Physical Review B **59**, 1758 (1999).

[72] A. Front, B. Legrand, G. Tréglia, and C. Mottet, Surface Science **679**, 128 (2019).

[73] A. Front and C. Mottet, The Journal of Physical Chemistry C **125**, 16358 (2021).